Chemical vapor detection with a multispectral thermal imager

Mark L. G. Althouse, MEMBER SPIE
U.S. Army Chemical Research
   Development and Engineering Center
SMCCR-DDT
Aberdeen Proving Ground, Maryland
   21010

Chein-I Chang, MEMBER SPIE
University of Maryland
Department of Electrical Engineering
Baltimore, Maryland 21228

Abstract. Detection of chemical vapors with a remote sensor is necessary for both military defense and civilian pollution control. The thermal imager is a natural instrument from which to build a chemical sensor since most chemical vapors of interest are spectrally active in its operating wavelength range. A system has been designed to place a chemical detection capability as an adjunct function in a military thermal imager. An additional detector array, which is spectrally filtered at the focal plane, is added to the imager. Real-time autonomous detection and alarm is also required. A detection system model by Warren, based on a Gaussian vapor concentration distribution is the basis for detection algorithms. Algorithms recursive in both time and spectral frequency have been derived using Kalman filter theory. Adaptive filtering is used for preprocessing clutter rejection. Various components of the detection system have been tested individually and an integrated system is now being fabricated.

CONTENTS

1. INTRODUCTION

Detection of chemical vapor clouds has been a military concern since the first use of chemical warfare. Growing concern for environmental pollution has additionally driven development of remote chemical vapor detectors.[1] The FLIR (forward looking infrared) is an 8- to 12-μm thermal imager widely used in the military for target acquisition and night vision. Chemical vapors are spectrally active in the 8- to 12-μm region. There have been several military programs to adapt the FLIR for chemical detection.[2-5] A navy FLIR has been deployed for chemical sensing.[4] It is a standard common module FLIR modified with bandpass spectral filters. Agent detection is made by the operator based on the viewed scene.

Army requirements specify an autonomous detection system not dependent on an operator for an alarm decision. To meet

that requirement, the Chemical Research, Development, and Engineering Center (CRDEC), as part of its detection program, is developing automatic image enhancement and detection algorithms. A large body of work exists on target detection and recognition in thermal images. But the targets of interest in this work are tanks, trucks, aircraft, and buildings, all objects that are generally modeled by such deterministic functions as shape and size. Vapor clouds fit no fixed size, shape, or motion categories, but rather are modeled statistically based on their concentration. The detection problem becomes one of deciding on the composite hypothesis of the image containing one or more distributions of various chemical vapors versus the hypothesis of the image containing only the clutter background. Additionally, any detection algorithm must operate in real time, that being the 1/30-s time period between the arrival of frames of video. To meet this constraint, adaptive and recursive realizations are pursued, as are parallel and pipelined implementations.

Since more sensitive remote detection methods exist for a dedicated chemical sensor, specifically IR interferometry[6] and laser spectroscopy,[7] the strengths of the FLIR-based approach are the pictorial output and the large numbers of standard FLIRs in use in the military. Because most tactical vehicles and aircraft are fitted with an FLIR, the space- and cost-economical way to provide them with a remote chemical vapor sensing capability would be through inclusion of that capability in the FLIR. As the next generation of FLIRs is developed, an adjunct chemical vapor detection capability could be incorporated as an optional configuration.

2. SENSOR CONCEPT

Turning an FLIR into a spectrometer using narrow-bandpass filters is a fairly simple process. Placing a filter in front of the

exit aperture of the FLIR, much as one does with a filter on a camera, is the initial solution. To get more than one spectral band requires the installation of a filter wheel or some mechanical device to change filters. Of course when the expense of IR filters several centimeters in diameter becomes apparent, a quick move is made to an internal focal point in the FLIR. This was the initial approach[8] at CRDEC and it performed well for proof of principle and initial trials. The stepper-motor-controlled filter wheel could reliably switch filters every second, at its fastest. Thus an entire set of four bands could be collected in about 10 s. Such a collection rate would be adequate for a fixed detector, i.e., nonmobile. To increase the data collection rate the next iteration chemical sensing FLIR has a continuously spinning filter wheel.[8,9] This wheel has three different passbands and is synchronized to the video frame rate of the FLIR, thus yielding a full set of spectral data every three frames or 1/10 s. A 0.1-s data collection time would be adequate in slowly moving vehicles. But this system still requires a fully dedicated FLIR and would experience too much registration error for use in aircraft.

Dividing the 8- to 12-μm region into smaller regions in an FLIR can be accomplished only with filters or a dispersion optic, both of which have transmission losses. Imaging spectrometers based on other principles exist but do not have the spatial resolution, compact size, or high-data-acquisition rate of the FLIR.[10] In the case of filters, the passband may be as narrow as 0.5 μm and still yield an 80% peak transmission. Filters smaller in passband quickly degrade in peak transmission. Although the filter decreases the total energy incident on the detector, thus lowering overall sensitivity, it has the advantage that an absorption feature located within the filter passband comprises a much larger percentage of the energy incident on the detector. This yields a better signal-to-noise ratio for the object with that absorption feature. Figure 1 illustrates two filter passbands and the spectrum of SF6, which has a spectral feature in the 10.6-μm filter passband.

There are two difficulties with using standard bandpass filters. To divide the 8- to 12-μm band fully into 0.5-μm-wide segments would require eight individual filters. These need to be mechanically rotated into the field of view sequentially to obtain spectral data over the full range. There could alternatively be eight to ten individually filtered detector arrays, each with a different passband, and some method for scanning the field of view over each detector array. Either system requires an optical redesign of the FLIR. A second difficulty is that the detector now views a "hot" (system operating temperature) filter element
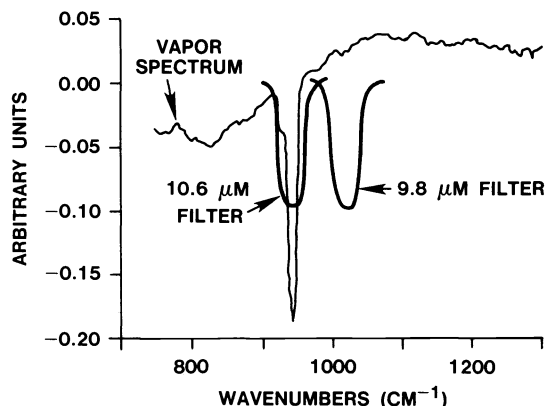
that is opaque over much of the sensitivity range of the detector. Out-of-passband emission from the filter represents a noise source. This may not be a problem if the scene background is significantly warmer than the filter, but if a colder scene is viewed, the warmer filter causes a considerable loss of sensitivity. Another concern specific to tactical military FLIRs is the requirement for excellent spatial resolution and good sensitivity for target acquisition and recognition. The image quality and operational availability of the tactical sensor cannot be compromised in any way by the addition of further mission requirements, such as chemical detection or hardware, such as filters. To address all of the necessary elements for adjunct chemical detection in a harmonious way leaves little space for design alternatives but does accommodate a solution.

3. HARDWARE DESCRIPTION

There is an arrangement that would permit the modified FLIR to deliver both its standard image and a filtered image simultaneously, which we call CSFLIR for chemical sensing FLIR. The standard image would not be degraded in any way. The filtered image would be designed to have the highest sensitivity obtainable for the given detector array and filter bands. Use of both the filtered and unfiltered images allows sufficient spectral characterization of the viewed scene to detect and classify chemical vapor clouds.

Figure 2 illustrates the focal plane filtering concept for a tactical FLIR. There are two detector arrays, the standard tactical one and a filtered one for chemical detection. The tactical array is a standard common module detector array, which is a linear array of semiconductor detector elements, generally 1×180, 1×120, or 1×60. The semiconductor material is HgCdTe for 8- to 12-μm detectors. Individual element sizes are on the order of 4×10^{-2} by 6×10^{-2} mm. The signals produced on these detector elements, as a scene is scanned over them, are electronically formed into a video image. Dual detector implementation in the common module FLIR would require a redesign of the Dewar assembly to accommodate additional electronic connections.

The chemical sensing detector array would be identical in construction techniques and material to the common module (CM) array. It could have elements the same size as or larger than the CM array. A larger detector element could be used because it is more sensitive (less noisy) than the small one. The trade-off is a loss of spatial resolution in the scene. This trade-off has been found not to be a great concern in vapor cloud sensing as vapor clouds tend to be large relative to the scene

Fig. 1. Simulant spectrum with passband of on-feature and off-feature spectral filters.
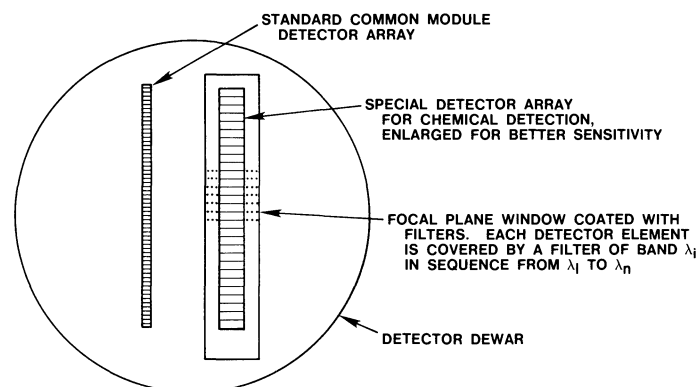

Fig. 2. Focal plane filtering concept.

and have indistinct edges. High-spatial resolution is necessary to resolve small objects or sharp edges in a scene.

A focal plane filter is mounted above the chemical detector array within the cooled detector housing. It consists of a window material, highly transmissive in the 8- to 12-μm band, coated with patches of narrow bandpass filter coatings. The bandpass filters are made by vapor depositing multiple layers of 1/4-wavelength thickness dielectric material on the window substrate. A wide variety of materials are used and the deposition process is well understood. Adjacent filter patches have different passbands. The number of distinct passbands required depends on the complexity and number of chemical vapors being detected. A passband should be associated with each strong absorption feature and at least one band where there are no features for baseline or background reference. The filter patches would be arranged in order from 1 to n, repeating the order till the whole detector array is covered, as shown in Fig. 3. The physical depth of some of the passband coatings is on the order of the CM array element dimensions. As such it may not be possible to put a filter patch over each element, but the elements would be grouped; say four elements under a patch, one element lost in the transition region from one patch to the next, then four more, and so on, as in Fig. 4. Any number of detector elements could be placed under the filter such that the filter coating edge should not interfere with the detector element acceptance angle. The smallest groupings and hence the largest number of filter strips is desirable to get the most complete multispectral coverage on the image. A custom array with larger detectors could be matched to the design constraints of the filter patches, as in Fig. 3. The filter patch should be at least three times as wide as it is deep for structural stability. A filter patch edge with no slope is preferable as the transition will then occupy less space on the image plane. Each filter element cannot have an edge of the filter patch within its acceptance angle without experiencing serious focusing and spectral errors. The filters should be mounted far enough from the detector to avoid large noise contributions due to forward scattering from small defects, which generally exist in the filter patches. This scattering is called the Stierwalt effect.[11-13]

Since the filters are fabricated from 1/4-wavelength thickness layers sequentially applied, any foreign material that adheres to the filter during fabrication will result in a feature as shown in Fig. 5. The bump created by the defect acts as a lens to focus stray radiation onto the detector.

Commercial infrared filters generally contain some of these defects. Because the filters are not generally mounted close to the detector, the defects have no effect. Through careful pro-
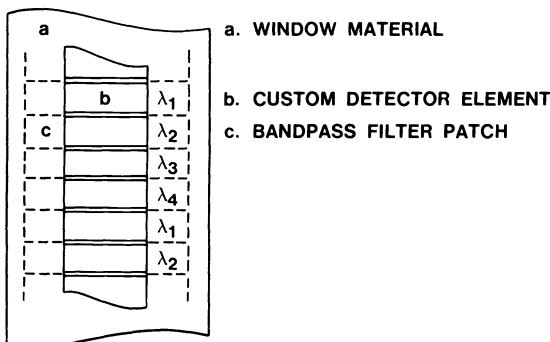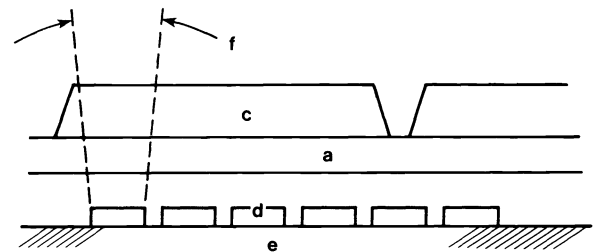

a. WINDOW MATERIAL
c. BANDPASS FILTER PATCH
d. COMMON MODULE DETECTOR ELEMENT
e. DETECTOR ASSEMBLY SUBSTRATE
f. ACCEPTANCE ANGLE

Fig. 4. Side view of a focal plane filter covering a common module detector array; four detector elements per filter patch.

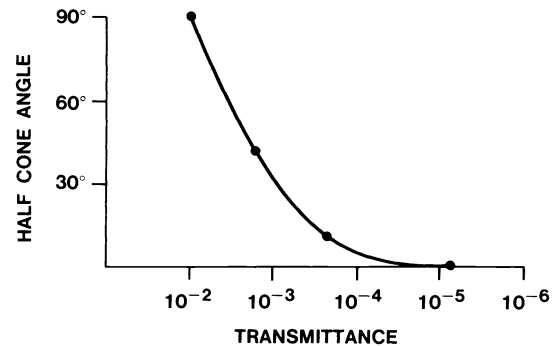**Fig. 5. Effect on filter coating layers due to a small particulate impurity.**

Fig. 6. Off passband transmittance from a spectral filter as a function of the half-cone angle of the detector.

cessing, we can greatly reduce the number of these defects and thus eliminate the consequent noise of the Stierwalt effect. Figure 6 shows some data from Stierwalt that illustrate the effect.[11] The curve shows transmittance of an out-of-passband frequency for various half-cone acceptance angles of the detector. As we move a filter with fixed aperture closer to the detector, the half-cone angle increases, to a limit of 90 deg. Figure 7 illustrates the change in half-cone angle with the change in offset distance of the filter from the detector for a fixed aperture. Defects in the filter coating not only scatter the object beam away from the detector, thus reducing desired signal strength, but scatter and focus stray radiation from outside the normal optical path and out-of-band radiation onto the detector, thus increasing the noise level. The larger the acceptance angle of the detector the more pronounced the effect.

Some recent measurements with high-quality filters indicated no Stierwalt effect up to a half-cone angle of 20 deg. Initial designs for a focal-plane-filtered FLIR include half-cone angles greater than 20 deg. As a result, great care is being taken to ensure a clean atmosphere and pure materials for the ongoing initial fabrication of these filters.

a. WINDOW MATERIAL
b. CUSTOM DETECTOR ELEMENT
c. BANDPASS FILTER PATCH

Fig. 3. Top view of a focal plane filter covering a custom detector array; one filter patch per detector element.
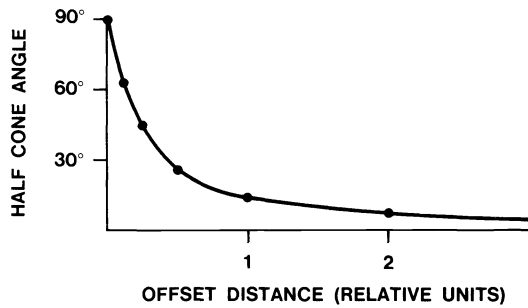
Fig. 7. Change in half-cone angle with varying offset distances for a fixed aperture 50% larger than the detector size. Units are normalized to the dimension of the detector.

The image resulting from the described chemical sensing detector would appear as in Fig. 8. Horizontal stripes of the image would be filtered by different passbands in a repeating order vertically down the image. A building or solid feature that has a flat emission spectrum would show only minor changes in appearance from stripe to stripe due to slightly unequal bandpass functions. On the other hand, the vapor cloud, which has distinct spectral properties, is strongly visible through filter 1, weakly visible through filter 3, and not visible through filters 2 and 4. To an operator this would be a very poor quality image, but to an image processor, its analysis poses no problem. Although the system does not produce a complete set of spectral data for each pixel, it does provide sufficient spectral analysis of the scene. RS-170 standard video is composed of 480 horizontal lines. Using the assumption of four filtered elements, the next element lost to filter patch transition, four more filtered elements, and so on, we would get 96 stripes in the image. The next generation of tactical FLIRs will have 480-line-image data. Given the 180-line CM display, we would get 36 stripes. With four distinct passbands, that would yield six complete filter sequences. Based on tests with vapor clouds generated in a realistic manner, the cloud quickly fills a significant portion of the image if it is close enough to be detected. The FLIRs used in the study had fields of view (FOV) on the order of 20×30 deg. Many tactical FLIRs have a much smaller FOV and thus will have the cloud fill a large portion of the FOV.

Another advantage of this system over the use of discrete filters in a filter wheel or a continuously variable filter is its
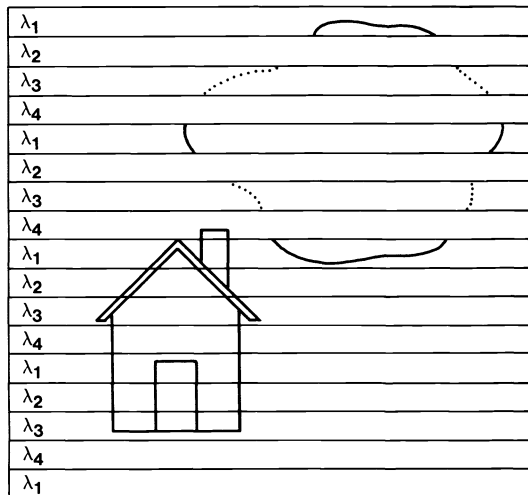
speed of data acquisition. Most image-processing techniques applicable to the cloud detection problem require good image stability and registration over the sequence of images used for analysis. Tactical FLIRs tend to be mounted on moving vehicles, resulting in motion in the scene between frames. Correcting the sensor motion is possible but computationally costly. In the new design both filtered and unfiltered images are collected simultaneously at the system frame rate, generally 30 Hz. The actual filtered pixel to corresponding unfiltered pixel collection time difference will be on the order of 10^{-5} s due to the physical separation of the detector arrays on the focal plane. For systems with a stepped filter wheel or continuously variable filter that same pixel collection time difference is on the order of seconds. In the case of the continuously spinning filter wheel, even this most ideal mechanically scanned system will have a pixel collection time difference of at least $1/30$ s. A 10^{-5} s time separation will keep any scene blurring at subpixel resolution even if the FLIR is mounted in a high-speed aircraft. Thus this system is compatible with present detection algorithms. The only improvement in the amount and usefulness of information collected would come from the addition of more detector arrays, each filtered at a single color, providing simultaneous multispectral data for each pixel.

The block diagram in Fig. 9 shows the major system components. The FLIR optics and tactical detector are as designed for a standard CM FLIR application. The CSFLIR detector and tactical detector are integrated into a detector/cooler assembly that includes a cryogenic pump. A data line from each detector carries the signal to video electronics modules that transfer it to RS-170 format. Both RS-170 lines feed a digital image processor. The image processor carries out the image enhancement routines called in the detection algorithm. Prior to the actual decision on the presence of a cloud, the detection algorithm controls the processing and extraction of relevant information contained in the available data.

Status of the chemical vapor detection operation is presented to the system operator via an audio or visual means. The operator could have manual selection of an appropriate display mode in his image display screen. It may be a colored area, shaded area, or perimeter overlay of the detected vapor cloud.
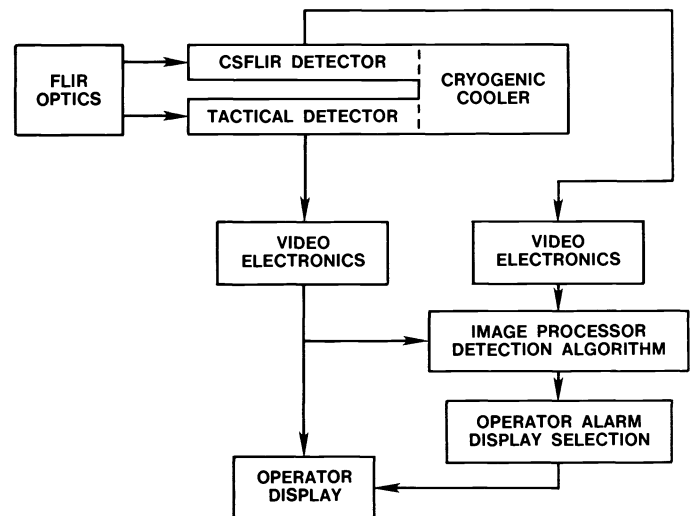

Fig. 8. Striped appearance of the filtered image.

Fig. 9. Major system components.

4. SYSTEM MODEL

For a standard target detection problem in the FLIR world, the target is a hard object that has a relatively fixed dimension and profile and produces a sharp-edged feature in the FLIR image. Detection algorithms of many types have been devised to separate features with those characteristics from the scene background or clutter.[14,15] Clutter itself is modeled as a first-order Markov process and statistical methods have been devised for its suppression.[16] Rauch et al. treated normal atmospheric clouds as clutter and investigated methods to suppress them.[17] Minor and Sklansky presented a method for detecting blobs, a class into which clouds can fall, in IR images using edge detection and other techniques designed for deterministically represented features.[18] We have found no other work in which clouds have been treated as a target for a detection algorithm. Since vapor clouds have certain properties that differ from clutter, even cloud clutter, these properties can be the basis of a discrimination technique.

In order to design a chemical agent detector for the multispectral FLIR, a sufficiently accurate system model is required. It must encompass the background, signal from the vapor cloud, and the sensor. The model described in this section is due to Warren.[19,20] We summarize briefly his derivation.

The extinction coefficient at wavelength λ

$$\epsilon_\lambda(\mathbf{x},z) = \epsilon_{a\lambda} + \rho_\lambda C(\mathbf{x},z) \ , \tag{1}$$

where $\mathbf{x} = (x,y)$ represents a two-dimensional spatial image, $\epsilon_{a\lambda}$ is an ambient atmospheric component, ρ_λ is the absorbtivity of the vapor, and $C(\mathbf{x},z)$ is the vapor concentration at location $\mathbf{x}$ in the plane at z, normal to the instrument line of sight. A Gaussian model for the vapor concentration is used:

$$C(\mathbf{x},z) = C_0 \exp\left[-\frac{(x^2+y^2+(z-z_0)^2)}{2\sigma_c^2}\right] \ ,$$

with C_0 the peak concentration and z_0 the cloud center. Since an FLIR, as a passive instrument, collects a signal integrated over the total path length, the path-integrated concentration $CL(\mathbf{x},z)$ is

$$CL(\mathbf{x},z) = \int_0^z C(\mathbf{x},z') \ dz' \tag{2}$$

$$= \sqrt{2\pi}C_0\sigma_c \exp\left[-\frac{(x^2+y^2)}{2\sigma_c^2}\right]\left[Q\left(-\frac{z_0}{\sigma_c}\right) - Q\left(\frac{z-z_0}{\sigma_c}\right)\right] \ , \tag{3}$$

with $Q(x)$ defined by

$$Q(x) = \int_x^\infty \exp(-t^2/2) \ dt \ .$$

The detected signal power P_d is a convolution of P_s, the power at the entrance aperture of the sensor, with R, the system point spread function,

$$P_d(\mathbf{x}_i) = \int P_s(\boldsymbol{\theta})R(\mathbf{x}_i/f - \boldsymbol{\theta}) \ d^2\boldsymbol{\theta} + P_n(\mathbf{x}_i) \ , \tag{4}$$

where $\mathbf{x}_i$ is the pixel location on the detector plane, $\boldsymbol{\theta}$ is the field of view direction of the pixel, f is the effective focal length, and P_n is the additive detector noise uncorrelated with the signal. Signal power P_d is considered a random function since both detector noise and the background temperature $T_B(\boldsymbol{\theta})$ are random functions. Thus we can characterize P_d by its first- and second-order moments. First we generalize Eq. (4) for a time (index k) series of multispectral (index j) images,

$$P_{dj}(\mathbf{x}_i,t_k) = \int P_{sj}(\boldsymbol{\theta},t_k)R(\mathbf{x}_i/f-\boldsymbol{\theta}) \ d^2\boldsymbol{\theta} + P_{nj}(\mathbf{x}_i) \ , \tag{5}$$

where the entrance aperture power is

$$P_{sj}(\boldsymbol{\theta},t_k) = A \int_0^\infty \left[F_j(\lambda)\left(B_\lambda(T_C) + \tau_A(\lambda) \exp[-\rho_\lambda CL(\boldsymbol{\theta},t_k)]\right.\right.$$

$$\left.\left.\times \{B_\lambda[T_B(\boldsymbol{\theta},t_k)] - B_\lambda(T_c)\}\right)\right] \ d\lambda \ . \tag{6}$$

Additional parameters are

A = system optical constant ,
$B_\lambda(T)$ = Planck function at temperature T,
$F_j(\lambda)$ = bandpass function of the optical filter centered at wavelength λ_j,
T_C = temperature of the vapor cloud, and
$\tau_A(\lambda)$ = transmittance of the atmosphere at wavelength λ.

The first and second moments of the signal power are

$$E[P_{dj}(\mathbf{x}_i,t_k)] \equiv \overline{P_{dj}(\mathbf{x}_i,t_k)} = \int E[P_{sj}(\boldsymbol{\theta},t_k)]R(\mathbf{x}_i/f-\boldsymbol{\theta}) \ d^2\boldsymbol{\theta} \tag{7}$$

and

$$\Lambda_{P_{dj'}}(\mathbf{x}_i,t_k,\mathbf{x}_{i'},t_{k'}) \equiv E\{[P_{dj}(\mathbf{x}_i,t_k) = \overline{P_{dj}(\mathbf{x}_i,t_k)}][P_{dj'}(\mathbf{x}_{i'},t_{k'})$$

$$- \overline{P_{dj'}(\mathbf{x}_{i'},t_{k'})}]\} \tag{8}$$

$$= \int [R(\mathbf{x}_i/f-\boldsymbol{\theta})\Lambda_{s_{jj'}}(\boldsymbol{\theta},t_k;\boldsymbol{\theta}',t_{k'})$$

$$\times R(\mathbf{x}_{i'}/f-\boldsymbol{\theta})] \ d^2\boldsymbol{\theta} \ d^2\boldsymbol{\theta}' \tag{9}$$

$$+ \Lambda_{n_{jj'}}(\mathbf{x}_i,t_k;\mathbf{x}_{i'},t_{k'}) \ , \tag{10}$$

where $1 \leqslant i \leqslant N^2$, $1 \leqslant k \leqslant M$, and $1 \leqslant j \leqslant L$.

Background or clutter temperature is assumed to be wide sense stationary such that $E[T_B(\boldsymbol{\theta},t_k)] = \overline{T}_B$, a constant. Although background scenes do not generally exhibit stationarity, Warren found that his algorithm performed well with field data. Using these two moments, the signal model is a multivariate Guassian density with signal power $\mathbf{P}_d$ expressed as an L-dimensional random vector $\mathbf{P}_d = (P_{d_1}, ..., P_{d_L})$ with probability density function given by

$$\mathscr{P}_{\mathbf{P}_d}(\mathbf{P}_d) = \frac{1}{(2\pi^{N^2ML}|\Lambda_{\mathbf{P}_d}|)^{1/2}}$$

$$\times \exp\left\{-\frac{1}{2}[(\mathbf{P}_d - \overline{\mathbf{P}_d})^T\Lambda_{\mathbf{P}_d}^{-1}(\mathbf{P}_d - \overline{\mathbf{P}_d})]\right\} \ . \tag{11}$$

Using the probability density function, Eq. (11), yields the following likelihood ratio test:

$$L(\mathbf{P}_d) = \frac{\mathscr{P}_{\mathbf{P}_d}(\mathbf{P}_d|H_T)}{\mathscr{P}_{\mathbf{P}_d}(\mathbf{P}_d|H_0)} \overset{H_T}{\underset{H_0}{\gtrless}} \frac{P(H_0)}{P(H_T)} \equiv \gamma \quad ,$$

where H_0 is the hypothesis that no vapor exists and H_T is the hypothesis that a vapor cloud target is present.

The above likelihood ratio can be further reduced to the summation over the time and spectral dimensions of a function $R_{kj}(\mathbf{x}_i)$, where $R_{kj}(\mathbf{x}_i)$ is arrived at by taking the product of the Fourier transform of each input image at each time increment and spectral frequency with the inverse of the autocovariance at each spectral frequency, the target filter function, and the sensor modulation transfer function (MTF). Here $R_{kj}(\mathbf{x}_i)$ is the result of the inverse Fourier transform of the above product. Computing the inverse of the autocovariance turned out to be the most time-consuming process. When implemented in FORTRAN on a MicroVAX computer, a 64-frame sequence of two spectral bands required more than ½ h to process. The resulting images had a very significant increase in signal-to-noise ratio and targets became easy to detect visually.[19]

5. PREPROCESSING ALGORITHMS: BACKGROUND CLUTTER SUPPRESSION

FLIR sensors image the thermal radiation emitted by a target. The target presence is identified by a difference in temperature between the target and the immediate surroundings, i.e., background clutter and noise. As a result, the loss of the contrast between the target and the background can seriously degrade the detectability of the target. In order to alleviate this problem, preprocessing is generally required prior to thresholding detection. Two preprocessing techniques are commonly used: (1) adaptive image enhancement[21] and (2) background suppression.[16,17,22,23] Of particular interest in multispectral images is the latter approach, which designs computationally efficient adaptive filters of different types to remove or suppress highly structured background clutter. Since an adaptive filter has the capability of adapting unknown statistics and yields desired results over a wide range of environments, the study of adaptive filters for a variety of applications has received considerable interest over the past years.[24]

A widely used technique for adaptive multispectral filtering is to use the minimum mean-square-error (MMSE) criterion to achieve background clutter suppression, thus improving detectability of targets in FLIR images.[16,17,23] The adaptive filter to be designed consists of a set of scalar filter coefficients expressed by a weighting vector $\mathbf{w}$. The output of the filter, $\mathbf{y}$ is the weighted sum of the input signal vector $\mathbf{x}$ given by

$$\mathbf{y} = \mathbf{w}^T \mathbf{x} \quad , \tag{12}$$

where T is the transpose and $\mathbf{w}$ is a weighting vector. An optimal adaptive filter is one minimizing the mean-square error between the desired signal and the output $\mathbf{y}$.

Two approaches to finding an optimal weighting vector for a desired MMSE adaptive multispectral filter are of interest.

5.1. Unconstrained MMSE adaptive filtering

FLIR image background suppression can be cast as an unconstrained MMSE adaptive filter problem.[16,17,23] The resulting optimal filter is generally referred to as a Wiener-Hopf filter. To be more specific, let $\mathbf{e}$ be the difference between the desired signals $\mathbf{s}$ and $\mathbf{y}$ expressed by

$$\mathbf{e} = \mathbf{s} - \mathbf{y} \quad . \tag{13}$$

An optimal filter minimizes the mean square of Eq. (13), i.e., $E(\mathbf{e}^2) = E[(\mathbf{s} - \mathbf{y})^T(\mathbf{s} - \mathbf{y})]$, where E is the expectation taken with respect to the joint random vector $(\mathbf{s}, \mathbf{y})$. The resulting optimal weighting vector $\mathbf{w}_{opt}$ is a solution to the well-known Weiner-Hopf equation:

$$\mathbf{w}_{opt} = \mathbf{R_x} \mathbf{D} \quad , \tag{14}$$

where $\mathbf{R_x}$ is the inverse of $\mathbf{M_x} = E[\mathbf{x}\mathbf{x}^T]$, the covariance matrix of $\mathbf{x}$, and $\mathbf{D} = E[\mathbf{x}\mathbf{s}]$ is the cross covariance matrix of $\mathbf{x}$ and $\mathbf{s}$.

We use a window (or search box) to implement adaptive filtering to suppress the background clutter of FLIR images. The window is moved and centered on all pixels in the image in turn to calculate all local covariance matrices. The window considered here is an adaptive filter specified by a weighting vector that puts weights on all pixels falling in the window. The details of implementation can be found in Refs. 16, 17, and 23.

5.2. Linearly constrained MMSE adaptive filtering

An alternative approach to the unconstrained MMSE adaptive filtering is a constrained MMSE adaptive filtering,[25] which is applied to the case where prior knowledge of the desired signal $\mathbf{s}$ is not known. Due to the lack of $\mathbf{s}$, a linear constraint vector $\mathbf{c}$ must be imposed on the filter to constrain the filter output. Let the linear constraint be given by

$$\mathbf{c}^T \mathbf{w} = g \quad . \tag{15}$$

The resulting constrained MMSE adapative filter is characterized by finding an optimal weighting vector $\mathbf{w}_{opt}$, a solution to the following equation:

$$\min_{\mathbf{w}}[\mathbf{w}^T \mathbf{M_x} \mathbf{w}] \quad \text{subject to } \mathbf{c}^T \mathbf{w} = g \quad , \tag{16}$$

where $\mathbf{w}_{opt}$ can be solved and given by

$$\mathbf{w}_{opt} = \frac{\mathbf{R_x}\mathbf{c}}{\mathbf{c}^T\mathbf{R_x}\mathbf{c}} g \quad . \tag{17}$$

Using the formulation (16), the adaptive filtering for FLIR background suppression can be accomplished by choosing an appropriate linear constraint vector $\mathbf{c}$ and a gain g. For instance, if we are interested in applying a 3×3 square array window to an image while maintaining the target signal unchanged, the gain g can be chosen to be unity and the constraint vector $\mathbf{c}$ chosen as a nine-dimensional vector with one in the central component and zero in all other components. As a result, the pixel falling in the center of the window is retained unchanged. This formulation yields a constrained MMSE problem. The resulting optimal filter is generally referred to as a minimum variance distortionless response (MVDR) adaptive beamformer.

5.3. Systolic array algorithms

A major difficulty encountered in the approaches described in Sec. 5.1 and 5.2 is the computation of the optimal weighting vector resulting from adaptive filters, which requires inverting

a sample covariance matrix $\mathbf{M_x}$ and intensive large-scale matrix/vector multiplications. It is very costly if the filter is implemented with direct matrix inversion. Although Wang[23] developed a recursive formula for generating the optimal weight vector to reduce computational load, full advantage of using matrix structures is not exploited.

Recently, the introduction of systolic array algorithms by Kung and Leiserson[26] revolutionized hardware design for carrying out matrix computations. With the help of systolic array algorithms, matrix computations can be performed in parallel and implemented in real-time processing. Basically, systolic array algorithms are orthogonal triangularization processes using QR-decomposition or Cholesky factorization, which allow us to triangularize the sample covariance matrix so that the resulting triangularized matrices can be inverted very efficiently by forward and backward substitutions. Most importantly, the systolic array algorithms are numerically stable, robust to finite arithmetic precision, and can be designed to be parallel and pipelined, thus greatly improving the implementation of the optimal filter in real-time applications. The details of studying such a systolic array approach are reported by Ref. 27.

6. REAL-TIME DETECTION ALGORITHMS

After preprocessing FLIR images, a thresholding technique is applied to detect the target signal. Many detection algorithms have been developed for this purpose. Among them is the detection algorithm suggested by Warren,[19,20] particularly noteworthy because it is recursive in time and has been shown to be effective.

Rather than following Warren's algorithm, which is based on a first-order autoregressive (AR) time series, Kalman filter theory is used to develop a similar recursive detection algorithm that covers Warren's algorithm as a special case and extends it to include recursion in spectral frequency. The idea of using a Kalman filter is natural since it can be recursively implemented in real-time processing. Unlike Warren's work, this approach uses a state equation to model background clutter of different types. The background clutter in Warren's work was assumed to be a first-order autoregressive model that corresponds to its counterpart, a state equation in Kalman filtering. Using the Markov property induced by the AR model, Warren derived a recursive formula for detectors described by a sequential likelihood ratio test statistic. The essence of Kalman filter theory is to introduce a new process, the innovations process suggested by Kailath.[28] Instead of directly dealing with an observation process, an innovations process is generated for updating new information as time goes along. In other words, given an observation process it is not necessary to store all information available up to the processing time because some information will be useless and some will be repeatedly stored, which wastes storage. A more efficient way to manage information is to store all necessary information only once and dump unnecessary or unwanted information. The innovations process is developed based on this need. In general, an observation process can be decomposed into two processes, a predicted process and an unpredicted process. The predicted process contains all previous information required for processing, and the unpredicted process presents new information available at the processing time but not contained in the predicted process. Such an unpredicted process resulting from the observation process is generally referred to as an innovations process.

In most practical cases, the background $B_k(\mathbf{x})$ at time frame k can be characterized by a first-order AR model (or state equation) given by

$$B_k(\mathbf{u}) = \gamma(\mathbf{x})B_{k-1}(\mathbf{x}) + n_k(\mathbf{x}) \quad , \tag{18}$$

and the observation process specified by a spatial image, sampled at time k is given by a random process $I_k(\mathbf{x})$. A standard detection problem can be described by a binary hypothesis-testing problem given as follows. At time frame k,

$$H_0: \quad I_k(\mathbf{x}) = B_k(\mathbf{x}) + N_k(\mathbf{x}) \tag{19}$$

versus

$$H_1: \quad I_k(\mathbf{x}) = T_k(\mathbf{x}) + B_k(\mathbf{x}) + N_k(\mathbf{x}) \quad , \tag{20}$$

where $T_k(\mathbf{x})$ is the target of interest and both $N_k(\mathbf{x})$ in Eqs. (19) and (20) and $n_k(\mathbf{x})$ in Eq. (18) are noises.

Instead of using $I_k(\mathbf{x})$ and $B_k(\mathbf{x})$, we can use two innovations processes $\alpha_k(\mathbf{x})$ and $\epsilon_k(\mathbf{x})$ to replace $I_k(\mathbf{x})$ and $B_k(\mathbf{x})$ in Eqs. (19) and (20), respectively, where $\alpha_k(\mathbf{x})$ and $\epsilon_k(\mathbf{x})$ are given by

$$\alpha_k(\mathbf{x}) \equiv I_k(\mathbf{x}) - \hat{I}_{k|k-1}(\mathbf{x}) \tag{21}$$

$$\epsilon_k(\mathbf{x}) \equiv B_k(\mathbf{x}) - \hat{B}_{k|k-1}(\mathbf{x}) \quad , \tag{22}$$

and both $\hat{I}_{k|k-1}(\mathbf{x})$ and $\hat{B}_{k|k-1}(\mathbf{x})$ are the estimates of $I_k(\mathbf{x})$ and $B_k(\mathbf{x})$ at time k and are obtained based on previous information up to time frame $k-1$. As a consequence, a detection problem using a Kalman filter with the state model, Eq. (18), can be derived and given by

$$H_0: \quad \alpha_k(\mathbf{x}) = s_{k|0}(\mathbf{x}) + \epsilon_k(\mathbf{x}) + N_k(\mathbf{x}) \tag{23}$$

versus

$$H_1: \quad \alpha_k(\mathbf{x}) = s_{k|1}(\mathbf{x}) + \epsilon_k(\mathbf{x}) + N_k(\mathbf{x}) \quad , \tag{24}$$

where $s_{k|0}(\mathbf{x}) = 0$ for H_0, no target present, and $s_{k|1}(\mathbf{x}) = T_k(\mathbf{x})$ for H_1, target present.

As we can see from the above, the innovations process $\alpha_k(\mathbf{x})$ is a process containing the new information available in the process $I_k(\mathbf{x})$ at time k but not in $\hat{I}_{k|k-1}(\mathbf{x})$, where $\hat{I}_{k|k-1}(\mathbf{x})$ is the predicted process obtained from the past information up to time $k-1$. Similarly, $\epsilon_k(\mathbf{x})$ is the innovations process representing the new information provided by the state model $B_k(\mathbf{x})$ at time k, but not available in the past. It is obtained by subtracting the predicted process $\hat{B}_{k|k-1}(\mathbf{x})$ from $B_k(\mathbf{x})$ so that the predicted information from $B_i(\mathbf{x})$ up to time $i = 0, \ldots, k-1$ can be removed. One of the most important features these two innovations processes possess is that they are white, i.e., independent processes. This is not true for the detection model of Eqs. (18) through (20) considered by Warren. The property of independency makes detection problems extremely easy to deal with. The observation of such independency is easily justified. Since an innovations process contains unpredicted new information obtained at different time frames, the information obtained at a certain time frame must be independent of other time frames due to the nature of unpredictability. The relationship between the two innovations processes can be demonstrated by the following equation:

$$\alpha_k(\mathbf{x}) = B_k(\mathbf{x}) + N_k(\mathbf{x}) - \hat{B}_{k|k-1}(\mathbf{x}) \qquad (25)$$

$$= \epsilon_k(\mathbf{x}) + N_k(\mathbf{x}) \ . \qquad (26)$$

Another great advantage of using a Kalman filter over Warren's approach is that the derived formula can be extended to more general models for background clutter other than AR models. The details of development of a Kalman-filter-based detection algorithm can be found in the report by Chang.[29]

Although algorithms to date are designed for a three-dimensional data set (pixel, time, spectral frequency), and the CSFLIR data will be more of the form [spectral frequency (pixel), time], separation of the spectral frequency function into its linear components is really a bookkeeping process. Comparison of adjacent components (really the horizontal stripes in the image) with the associated unfiltered pixels provides a sufficiently complete set of data due to the correlation between neighboring pixels.

7. CONCLUSIONS

Remotely detecting chemical vapors with a thermal imager has proven to be a viable technique. Operational constraints drive the degree of modification necessary to convert a standard FLIR into a chemical sensor. The developmental FLIR design presented here would yield a compact multipurpose electro-optical system for obtaining multispectral imagery from a moving platform. The multispectral data would be stationary and complete enough for the planned detection algorithms. Hardware technical issues, such as scattering from defects in the filters, exist but have engineering solutions and require no new science.

Detection algorithm work accomplished to date suggests a real-time solution to autonomous operation. Adaptive filtering for clutter rejection and recursive realizations of thresholding detectors must be further refined with realistic data and then implemented on systolic array and parallel hardware. Additionally, neural networks may perform well for circumstances where little or no prior knowledge of the target exists.

The potential applications of this technique are not limited to chemical vapor detection or remote sensing. Any scene that contains hard to resolve or differentiate objects that also have spectral features distinct from the background can be analyzed by an imager such as the one described here. Some examples are medical imaging or industrial process control. It is also possible to extend the spectral range beyond the 8- to 12-μm region used in this description. The constraints come from the limited spectral bands of optical components, but the use of all or nearly all reflective optics is helpful. More than the two detectors shown in this description may also be used to adequately cover the spectral range needed.

8. ACKNOWLEDGMENTS

9. REFERENCES

1. G. W. Small, et al., "Detection of atmospheric pollutants by direct analysis of passive Fourier transform infrared interferograms," *Anal. Chem.* 60, 264–269 (1988).
2. H. Walter, Jr. and D. Flanigan, "Detection of atmospheric pollutants: a correlation technique," *Appl. Opt.* 14(6), 1423–1428 (1975).
3. T. T. Accord, et al., "Common module imaging spectral radiometer,"
   Report DELNV-TR-0021, U.S. Army Night Vision and Electro-Optics Laboratory (1981).
4. B. Vastag, et al., Report NSWC-TR-84-425, Naval Surface Weapons Center, Dahlgren, Va. (1984).
5. M. L. G. Althouse, "Spectral filtering of thermal imagers for gas detection," *Proc. 3rd Int. Symp. Protection Against Chemical Agents*, pp. 143–148, Umea, Sweden (June 1989).
6. D. F. Flanigan, "Detection of organic vapors with active and passive sensors," *Appl. Opt.* 25(23), 4253–4260 (1986).
7. K. R. Phelps and M. L. Althouse, "Chemical agent remote sensing," Proc. SPIE 783, 185–189 (1987).
8. L. Carr, et al., "Characterization of filtered FLIR systems designed for chemical vapor detection and mapping," Proc. SPIE 1309, 90–103 (1990).
9. P. L. Holland, L. W. Carr, L. D. Fletcher, M. L. G. Althouse, and G. L. Doggett, "1988 thermal imager field test report," Report CRDEC-CR-056, U.S. Army Chemical Research, Development and Engineering Center, Aberdeen Proving Ground (1989).
10. I. B. Breckinridge, et al., "Reflecting Schmidt Imaging Spectrometers," *Appl. Opt.* 22(8), 1175–1180 (1983).
11. D. L. Stierwalt, "Geometrical effects on the out of band transmittance of interference filters," *Opt. Eng.* 13(3), G115–G117 (1974).
12. T. W. Merritt, J. V. Gavin, and C. A. Burke, "Spectral characterization methodology of thin film optical filters," Proc. SPIE 308, 54–55 (1981).
13. K. H. Guenther, "Nodular defects in dielectric multilayers and thick single layers," *Appl. Opt.* 20(6), 1034–1038 (1981).
14. B. Bhanu and R. D. Holben, "Model based segmentation of FLIR images," *IEEE Trans. Aerospace Electronic Systems* 26(1), 2–10 (1990).
15. A. D. Gross and A. Rozenfeld, "Multiresolution object detection and delineation," *Comput. Vision, Graphics, and Image Processing* 39, 102–115 (1987).
16. A. Abridges, G. Cook, S. Mansur, and K. Zonca, "Correlated background adaptive clutter suppression and normalization techniques," Proc. SPIE 933, 32–44 (1988).
17. H. E. Rauch, W. I. Futterman, and D. B. Kemmer, "Background suppression and tracking with a staring mosaic sensor," *Opt. Eng.* 20(1), 103–110 (1981).
18. L. G. Minor and J. Sklansky, "The detection and segmentation of blobs in infrared images," *IEEE Trans. Sys. Man. Cyber.* SMC-11(3), 194–201 (1981).
19. R. E. Warren, "Algorithm for the image enhancement and detection of chemical vapors using a thermal imager," Report CRDEC-CR-018, U.S. Army CRDEC, Aberdeen Proving Ground, Md. (1989).
20. L. Carr, D. McPherrin, and R. Warren, "Low contrast detection algorithm," U.S. Army CRDEC contract DAAA15-86-C-0109, SRI International, Menlo Park, Calif. (1990).
21. T. Peli and J. S. Lim, "Adaptive filtering for image enhancement," *Opt. Eng.* 21(1), 108–112 (1982).
22. T. F. Tao, D. Bar-Yehoshua, B. Evenor, and J. Adkins, "Statistical nonrecursive spatial filter for processing of infrared mosaic sensor images," in *Modern Utilization of Infrared Technology*, Proc. SPIE 156, 10–19 (1978).
23. D. Wang, "Adaptive spatial/temporal/spectral filters for background clutter suppression and target detection," *Opt. Eng.* 21(6), 1033–1038 (1982).
24. S. Haykin, *Adaptive Filter Theory*, second ed., Prentice-Hall, Englewood Cliffs, N.J. (1991).
25. O. L. Frost III, "An algorithm for linearly constrained adaptive array processing," Proc. IEEE 60, 926–935 (1972).
26. H. T. Kung and C. E. Leiserson, "Systolic arrays for VLSI," *Sparse Matrix Proc. SIAM*, pp. 256–282 (1978).
27. C.-I Chang and M. Althouse, "VLSI systolic array architectures of adaptive spatial filtering for FLIR target detection," *Proceedings of IEEE Workshop on Visual Signal Processing and Communications*, June 6–7, Taipei, Taiwan, pp. 110–115 (1991).
28. T. Kailath, "An innovations approach to least-squares estimation: Part 1. linear filtering in additive white noise," *IEEE Trans. Automatic Control* AC-13, 646–655 (1968).
29. C.-I Chang, *Implementation Scheme for Recursion in Spectral Dimension*, Report, U.S. Army CRDEC, Contract DAAD-05-90-P8392, University of Maryland, Baltimore, Md. (1991).

Mark L. G. Althouse received his BS in physics from the Pennsylvania State University in 1981, his MS in electrical engineering from Johns Hopkins University in 1988, and is presently working on his Ph.D. at the University of Maryland. Since 1981 he has been employed by the U.S. Army Chemical Research Development and Engineering Center, Aberdeen Proving Ground, Maryland, working on the remote detection of chemical and biological agents. From 1985 to 1986 he was an exchange scientist at the German NBC Defence Laboratory in Munster, Germany. Mr. Althouse is a member of OSA, SPIE, IEEE, and INNS. He is also a member of the OSA Education Council.

Chein-I Chang received his BS, MS, and MA degrees from Soochow University, Taipei, Taiwan in 1973, National Tsing Hua University, Hsinchu, Taiwan in 1975, SUNY at Stony Brook in 1977, respectively, all in mathematics; and MSEE from the University of Illinois at Urbana-Champaign in 1982, Ph.D. in electrical engineering from the University of Maryland, College Park, in 1987. From 1973 to 1977 he was a teaching assistant at Soochow University, National Tsing Hua University and SUNY at Stony Brook. From 1977 to 1980 he was an instructor of mathematics at the University of Illinois. During 1980 and 1982 he was a research assistant at the University of Illinois and was also a research assistant at the University of Maryland from 1982 to 1986. He was Visiting Assistant Professor in the College of Engineering at the University of Maryland, Baltimore County campus, from January to August 1987, where he is currently Assistant Professor of electrical engineering. His research interests include information theory, signal detection and estimation, digital signal/image processing, and adaptive signal processing. Dr. Chang is a member of Phi Kappa Phi and Eta Kappa Nu.